Journal of Materials Chemistry C

PAPER

View Article Online
View Journal | View Issue

Cite this: J. Mater. Chem. C, 2016, 4, 11198

Role of rare earth ions in the magnetic, magnetocaloric and magnetoelectric properties of $RCrO_3$ (R = Dy, Nd, Tb, Er) crystals†

L. H. Yin,*[a] J. Yang,[a] P. Tong,[a] X. Luo,[a] C. B. Park,[b] K. W. Shin,[b] W. H. Song,[a] J. M. Dai,[a] K. H. Kim,[b] X. B. Zhu[a] and Y. P. Sun*[acd]

Received 16th September 2016,
Accepted 1st November 2016

DOI: 10.1039/c6tc03989h

www.rsc.org/MaterialsC

We report a systematic study on the magnetic, magnetocaloric (MC), specific heat and magnetoelectric (ME) properties of the single crystals of rare-earth orthochromites, $RCrO_3$ (R = Dy, Nd, Er, Tb). Interesting stair-like metamagnetic transitions were observed for the first time in $TbCrO_3$ crystals. Intrinsic large anisotropy in the magnetic and ME properties were also revealed in all of the $RCrO_3$ crystals. The reorientation/ordering of the rare earth R^{3+} spins was observed to be accompanied with large MC, rotating MC and ME effects. These behaviors are found be closely related to the R–R and R–Cr interactions in these chromites. In particular, the ME effect can be ascribed to the spin–phonon coupling. All these results suggest the essential and unique role of 4f electrons of rare earth ions in these chromites.

1 Introduction

Rare earth elements R with 4f electrons are vital to modern technologies due to their unique magnetic, luminescent and electrochemical properties.[1,2] The electrons in the partially occupied 4f shell contribute to the unique magnetic moment of rare earth ions and enable compounds containing rare earth elements to show various intriguing physical properties. Nd and Sm are usually used in permanent magnets.[3] Gd metal or Gd-based alloys are the typical working materials used for magnetic refrigeration based on large magnetocaloric (MC) effects.[2,4] It has also been found that the magnetic interaction between rare earth ions and 3d transition metal ions plays an important role in the MC, magnetoelectric (ME) effect and multiferroic properties in the rare earth orthoferrites, $RFeO_3$, and manganites, $RMnO_3$ (R = Dy, Gd, *etc.*).[5–7]

Among the rare earth based compounds, the rare earth orthochromites $RCrO_3$, with a simple perovskite structure, in which R–R, R–Cr and Cr–Cr magnetic interactions coexist, exhibit unique interesting phenomena. The typical crystallographic and spin structures following Bertaut's notation[8] for $RCrO_3$ systems are shown in Fig. 1. In fact, exotic magnetism, like temperature induced magnetization reversal and temperature induced magnetization jump, has been observed in $RCrO_3$ and doped $RCrO_3$ systems.[9–12] ME and multiferroicity arising from R–Cr interactions or disorder effects were also reported in $RCrO_3$ and $YCr_{1-x}M_xO_3$ (M = Fe, Mn) systems;[13,14] however, later reports on the multiferroicity in $LuCrO_3$ with non-magnetic rare earth Lu suggest a contrasting origin of

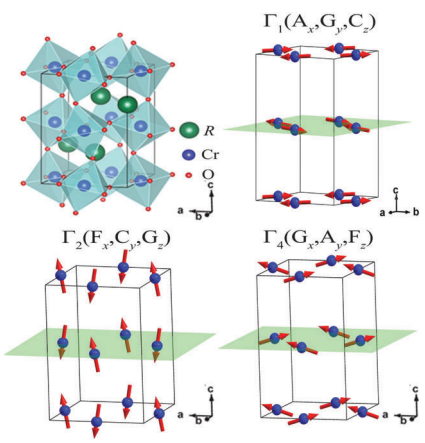

Fig. 1 Schematic view of the crystal structure and typical spin configurations for the $RCrO_3$ systems.

[a] Key Laboratory of Materials Physics, Institute of Solid State Physics, Chinese Academy of Sciences, Hefei 230031, People's Republic of China. E-mail: ypsun@issp.ac.cn, lhyin@issp.ac.cn; Fax: +86 551 6559 1434; Tel: +86 551 5592757

[b] Center for Novel States of Complex Materials (CeNSCMR) and Institute of Applied Physics, Department of Physics and Astronomy, Seoul National University, Seoul 151-747, Korea

[c] High Magnetic Field Laboratory, Chinese Academy of Sciences, Hefei 230031, People's Republic of China

[d] Collaborative Innovation Center of Advanced Microstructures, Nanjing University, Nanjing 210093, People's Republic of China

† Electronic supplementary information (ESI) available: Specific heat data of $RCrO_3$ (R = Dy, Nd, Er) crystals; more detailed magnetic properties (M–T) of $ErCrO_3$ crystals; MC properties of $GdCrO_3$ crystals; the Arrott plots of low temperature M–H curves for $NdCrO_3$ and $ErCrO_3$ crystals; magnetodielectric properties of $TbCrO_3$ crystals. See DOI: 10.1039/c6tc03989h

multiferroicity in these chromites.[15] Recently, it was reported that the ferroelectricity even survived at a temperature much higher than the antiferromagnetic (AFM) ordering temperature T_N of the Cr sublattice in both $HoCrO_3$ ceramics and films.[16] Furthermore, the $RCrO_3$ systems also show a large MC effect at low temperatures.[9,17] However, most of the above mentioned properties were reported for polycrystalline samples synthesized using solid state reaction,[13] hydrothermal[18] or solvothermal[10] methods, in which the magneto-crystalline anisotropic effect is not considered and the existence of a grain boundary may also bring in the grain size effect or other extrinsic effects.[19] Therefore, a single crystal is needed to clarify these problems. Furthermore, the ME properties at temperatures below the ordering of rare-earth spins are still lacking in chromites as compared to isostructural multiferroic $RFeO_3$ systems.[5,6]

In this article, we report the magnetism, MC and ME effects in the $RCrO_3$ (R = Dy, Nd, Er, Tb) chromite single crystals synthesized *via* the flux method. We observed new interesting phenomena like stair-like metamagnetic transitions and reorientation/ordering of rare earth spins. Strong anisotropic magnetism, MC and ME effects related to the R–R and R–Cr magnetic interactions were also observed in these chromite crystals.

2 Experimental

The $RCrO_3$ (R = Dy, Tb, Er) single crystals were grown using the flux method as reported previously.[20] The initial materials R_2O_3, Cr_2O_3, PbF_2, PbO, and B_2O_3 were mixed in a molar ratio of 1 : 1 : 8 : 2 : 1, placed into a platinum crucible, covered with a lid, and heated at 1200 °C for 4 days. After this, the mixture was cooled slowly to 1000 °C at a rate of 5 °C h^{-1}, and then the furnace was turned off. The $GdCrO_3$ crystals are the crystals used in our previous work[9] and detailed information on the growth of the $GdCrO_3$ and $NdCrO_3$ crystals is described in ref. 9.

The phase purity and structure of the obtained single crystals were confirmed using powder X-ray diffraction (XRD) (Philips diffractometer with Cu K_α radiation) at room temperature. The orientation of the crystals was determined according to the XRD of the natural major crystal faces, magnetic measurements and the results of previous reports.[21] The chemical composition of the crystals was analyzed using an energy dispersive spectroscopy (EDS) technique. The result agrees well with those expected from the chemical formula.

The magnetic measurements were carried out in a Quantum Design superconducting quantum interference device (SQUID) magnetometer. Temperature dependent magnetization data were collected in the field-cooled cooling (FCC) and field-cooled warming (FCW) processes. The dielectric measurements were performed using an LCR meter (TH2828S) at a frequency of 300 kHz with the temperature and magnetic field regulated by the Quantum Design Physical Property Measurement System (PPMS). The temperature dependent specific heat $C_P(T)$ was measured using the Quantum Design PPMS using a thermal relaxation method.

3 Results and discussions

Fig. 2 shows the temperature dependent magnetization (M–T) under the FCW mode along three major crystallographic axes

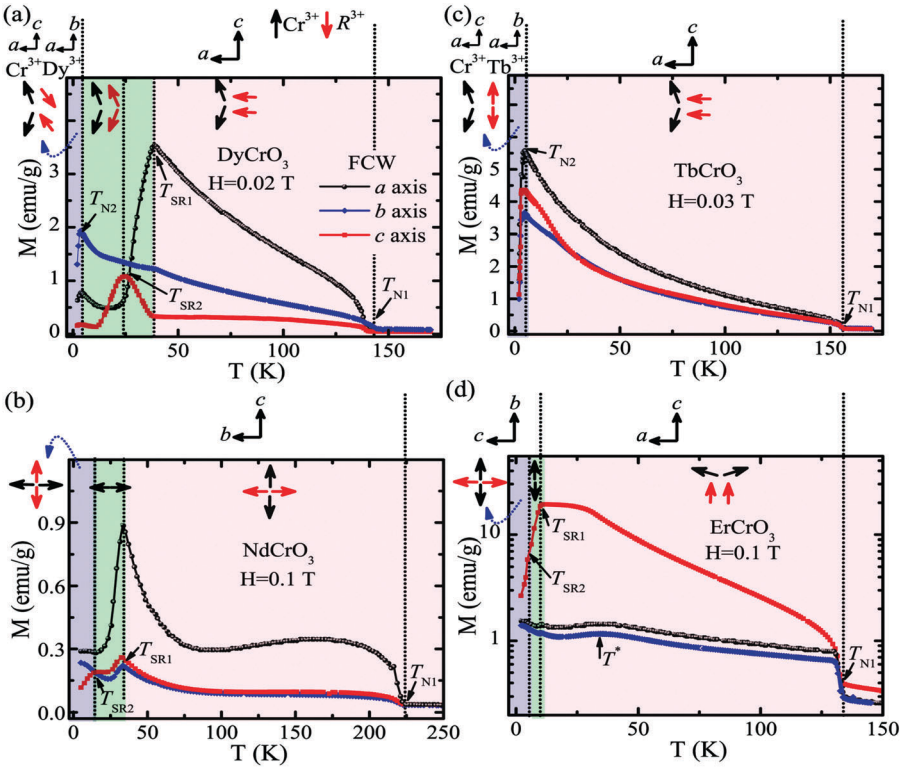

Fig. 2 Temperature dependence of magnetization and the corresponding schematic spin structure evolution along different axes for $RCrO_3$ crystals.

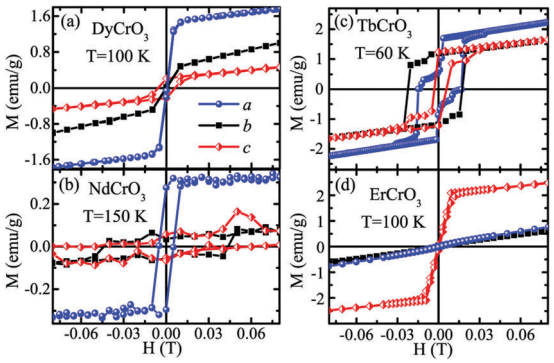

Fig. 3 Isothermal magnetic field dependence of magnetization along different axes for $RCrO_3$ crystals.

for the $RCrO_3$ (R = Dy, Nd, Tb, Er) single crystals. It is clear that all the crystals show strong magnetic anisotropy below the AFM ordering temperature T_{N1} of the Cr^{3+} spins. The magnetic field dependent magnetization (M–H) along the three different axes (Fig. 3) also exhibits strong anisotropy with the largest moment along the a axis for R = Dy, Nd, Tb and along the c axis for R = Er, which are in agreement with the spin configuration of the Cr^{3+} sublattice below the T_{N1} reported previously for these crystals.[21] The spins of rare earth R = Dy^{3+} and Tb^{3+} were ordered at low temperatures $T_{N2} \sim 3.8$ K and 5.0 K, respectively, while Nd^{3+} and Er^{3+} showed no long-range ordering at temperatures as low as 2 K, as shown in Fig. 2. Among all the titled compounds, long-range spin reorientation of the Cr^{3+} sublattice below the T_{N1} was only observed in $NdCrO_3$ and $ErCrO_3$ at $T_{SR1} \sim 33.5$ K and 10.2 K, respectively, consistent with a previous report.[21] The AFM transition temperature T_{N1}, together with the other characteristic magnetic phase transition temperatures for these crystals, are listed in Table 1.

In addition to the above-mentioned magnetic transitions reported previously, we also found some new features in these crystals. For the $DyCrO_3$ crystal, it was reported that the Dy^{3+} spins were polarized to be along the a axis below T_{N1} and lay in the basal plane at an angle of $\pm 63^\circ$ relative to the a axis below T_{N2}.[22,23] In the present work, we observed an additional, rather strong magnetic peak at $T_{SR1} \sim 39.2$ K and $T_{SR2} \sim 24.8$ K along the a and c axes, respectively, as shown in Fig. 2a. This behavior was not reported previously, which might be due to different sample preparation conditions. To obtain knowledge about the origin of these two magnetic peaks, the M–T curves along the a (M_a) and c (M_c) axes at different H were also recorded and are displayed in Fig. 4. Both peaks become weaker and tend to vanish at high H. The specific heat $C_p(T)$ does not show any anomaly around either T_{SR}* or T_{SR}, indicating the absence of long-range spin ordering or structure transitions (Fig. S1 of ESI†). Another feature is that the magnetizations M_a and M_c begin to decrease and increase, respectively, at T_{SR1} simultaneously, and M_c reaches a maximum at T_{SR2}. These results clearly show that the two peaks should be related to the reorientation of Dy^{3+} spins induced by the internal effective field of the Cr^{3+} sublattice. The Dy^{3+} spins begin to reorient from the a axis to the c axis at T_{SR1} and end in an AFM arrangement along the c axis at T_{SR2}. The evolution of the spin configuration for both the Cr^{3+} and Dy^{3+} sublattices are schematically plotted in Fig. 2a.

Similar to the case of $DyCrO_3$, an induced reorientation/ordering of the Nd^{3+} and Er^{3+} spins were also observed for the $NdCrO_3$ and $ErCrO_3$ crystals around $T_{SR} \sim 17.1$ K and 6.0 K (Fig. 2b and d), respectively, near which no anomaly was observed in specific heat (see Fig. S1 of the ESI† and ref. 24). The corresponding spin evolution of the R^{3+} and Cr^{3+} ions with the temperature for $NdCrO_3$ and $ErCrO_3$ is shown in Fig. 2b and d, respectively. For $NdCrO_3$, the decrease in M_c and increase in M_a occur simultaneously near T_{SR2}, and the peak at T_{SR2} in the M_c–T curve did not vanish even at $H \sim 3$ T (Fig. 5), in contrast to that in $DyCrO_3$. Another rather interesting phenomenon is the multi-step rise in the M–H curves along the a axis in $TbCrO_3$ (see Fig. 3c and 6), which was not reported previously. The initial M–H curve was recorded after cooling from above T_{N1} to 130 K under zero H (see Fig. 6). The overlap between the initial curve and the following hysteresis loop implies that the step-rise behavior is intrinsic rather than the domain effect. The multi-step behavior can be explained as the relative orientation variation of the Tb^{3+} and Cr^{3+} spins under H, which is schematically shown in Fig. 6.

For $ErCrO_3$, the anomaly around T_{SR2} in the M_c–T and M_a–T curves becomes weak at high H (Fig. S2 and S3 of ESI†), consistent with the H-induced phase transition from Γ_1 to Γ_4.[24] Another feature for $ErCrO_3$ is the relatively broad peak in the M_b–T and M_a–T curves at low H in the vicinity of $T^* \sim 34.7$ K, while no obvious anomaly near T^* was observed in M_c–T and specific heat (Fig. 2d and Fig. S1 of ESI†). This behavior is an indication of the possible induced reorientation of Er^{3+} spins near T^*. It should be noticed that the relative broad peak in the M–T curves around $T \sim 22$ K is usually observed in polycrystalline samples and wrongly ascribed to the SR of Cr^{3+},[13,25,26] which should actually be the combined and average

Table 1 Magnetic parameters including magnetic phase transition temperatures, maximum values of the MC effect, refrigerant capacity and rotating MC effect for $RCrO_3$ crystals. Some of the data for $GdCrO_3$ was adapted from ref. 9

					$-\Delta S_M$ (J kg^{-1} K^{-1})			$-\Delta S_M^R$ (J kg^{-1} K^{-1})		
Materials	T_{N1} (K)	T_{N2} (K)	T_{SR1} (K)	T_{SR2} (K)	ΔH = 2 T	ΔH = 4.5 T	RC (J kg^{-1})	ΔH = 2 T	ΔH = 4.5 T	Rotation mode
$DyCrO_3$	140.0	3.8	39.2	24.8	11.5	15.2	300	11.4	14.8	From c to b
$NdCrO_3$	222.5	—	33.5	17.1	−0.2	−1.1	—	—	—	—
$TbCrO_3$	156.0	5.0	—	—	5.0	12.2	125	0.7	5.4	From c to b
$ErCrO_3$	132.8	—	10.2	6.0	10.1	20.6	276	9.5	16.9	From b to c
$GdCrO_3$	166.0	—	7.0	—	14.1	31.6	—	4.3	3.8	From a to c

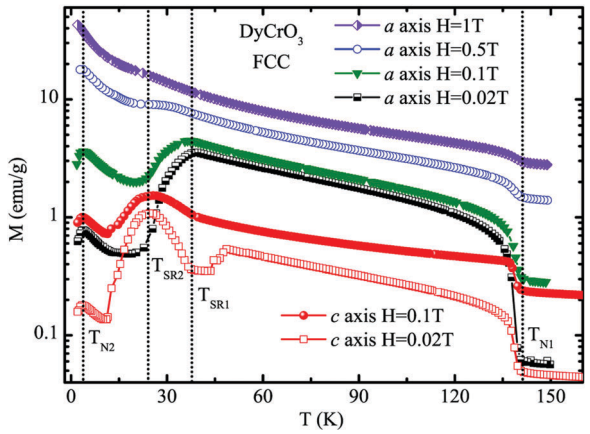

Fig. 4 Temperature dependence of magnetization along the *a* and *c* axes under different *H* for $DyCrO_3$ crystals.

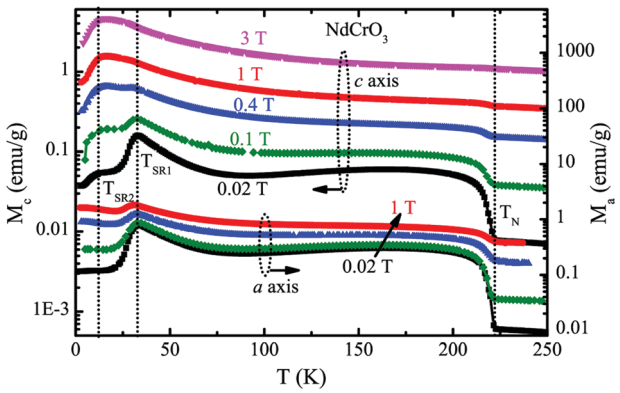

Fig. 5 Temperature dependence of magnetization along the *a* and *c* axes under different *H* for $NdCrO_3$ crystals.

effect of the SR at T_{SR1} and the anomaly near T^* observed in the single crystal in the present work.

Now let's turn to the MC effect. For the *M* obtained at a constant temperature at discrete *H* intervals, the magnetic entropy change $-\Delta S_M$ can be estimated by using the following equation based on the Maxwell relation:

$$\Delta S_M(T,H) = \int_0^H \left(\frac{\partial M}{\partial T}\right)_H dH = \sum_i \frac{M_{i+1} - M_i}{T_{i+1} - T_i}\Delta H_i \qquad (1)$$

where M_{i+1} and M_i are the experimental values of magnetization measured with a field H_i at temperatures T_{i+1} and T_i, respectively. Here the *M*–*H* curves were corrected by considering the demagnetization factor of the crystal. $-\Delta S_M$ along different axes for different field variations ΔH can be derived from the isothermal *M*–*H* curves and is displayed in Fig. 7. Here, the MC effect for the *a* axis is not shown due to the fact that its value is between that of the *b* and *c* axes. The largest value of $-\Delta S_M$ with ΔH = 2 T is 11.5 J kg^{-1} K^{-1} at T = 4.5 K for the $DyCrO_3$ crystal among all the titled compounds. The largest values of $-\Delta S_M$ with ΔH = 2 T and 4.5 T for $RCrO_3$ (R = Dy, Nd, Er, Tb) crystals are listed in Table 1. For comparison, the $-\Delta S_M$ for $GdCrO_3$ crystals along different axes are also listed in Table 1

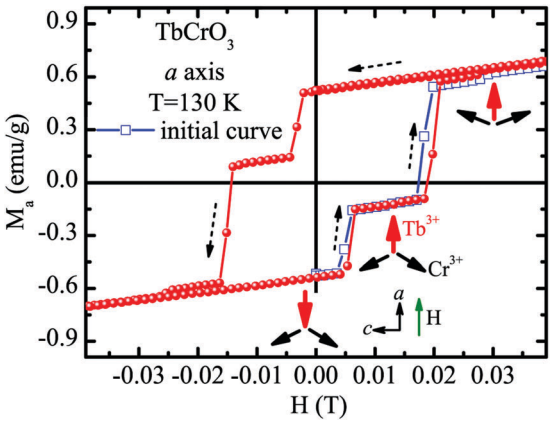

Fig. 6 Isothermal magnetization along the *a* axis at 130 K and the corresponding schematic spin structure evolution for $TbCrO_3$ crystals.

(see also Fig. S4 of the ESI†). It can be seen that the strong anisotropy in the *M*–*H* curves usually gives rise to a large anisotropic $-\Delta S_M$, as shown in Fig. 7. This anisotropic $-\Delta S_M$ suggests a large rotating MC effect in these crystals. The rotating MC effect can be expressed by the equation,[27]

$$-\Delta S_M^R = -(\Delta S_M(\theta) - \Delta S_M(90^\circ)) \qquad (2)$$

where θ is the angle between the easy magnetic axis and *H*, $\theta = 90^\circ$ denotes *H* applied along the hard axis. Therefore, in the case of the $DyCrO_3$ crystal, if *H* is initially applied along the *c* axis, and then the crystal is rotated isothermally by 90° to the *b* axis at a constant *H*; then this process will give rise to the isothermal rotating MC effect, which can be expressed as $-\Delta S_M^R = \Delta S_M(H\|c) - \Delta S_M(H\|b)$ at a certain temperature. The largest value of $-\Delta S_M^R$ thus obtained reaches 11.4 J kg^{-1} K^{-1} at 4.5 K and 14.8 J kg^{-1} K^{-1} at 8.5 K for ΔH = 2 T and 4.5 T, respectively (Table 1). And an even larger $-\Delta S_M^R \sim 16.9$ J kg^{-1} K^{-1} for ΔH = 4.5 T was obtained in the $ErCrO_3$ crystal. These values are much larger than those for manganite crystals such as $DyMnO_3$[28] and $HoMn_2O_5$,[29] and are even larger than those for the $KEr(MoO_4)_2$ crystals,[30] although smaller than those for the $DyFeO_3$ crystals.[31]

Another important factor for magnetic refrigeration is the magnetic cooling efficiency of a magnetic refrigerant material, *i.e.*, refrigerant capacity (RC). The RC is a measure of the amount of heat transfer between the hot and cold sinks in an ideal refrigeration cycle, and it can be evaluated by considering the magnitude of ΔS_M and its full-width at half-maximum as[4]

$$RC = \int_{T_1}^{T_2} |\Delta S_M| dT \qquad (3)$$

where T_1 and T_2 are the temperatures corresponding to both sides of the half-maximum value of the peak, respectively. The maximum values of RC for a field change of 4.5 T for all the titled crystals are listed in Table 1. The largest RC of $\sim$300 J kg^{-1} was obtained for the $DyCrO_3$ crystal along the *b* axis, which is also larger than those of the rare-earth manganite crystals such as $DyMnO_3$[28] and $HoMn_2O_5$.[29]

It should be noted here that all the titled compounds experience a peak in the vicinity of the ordering or induced

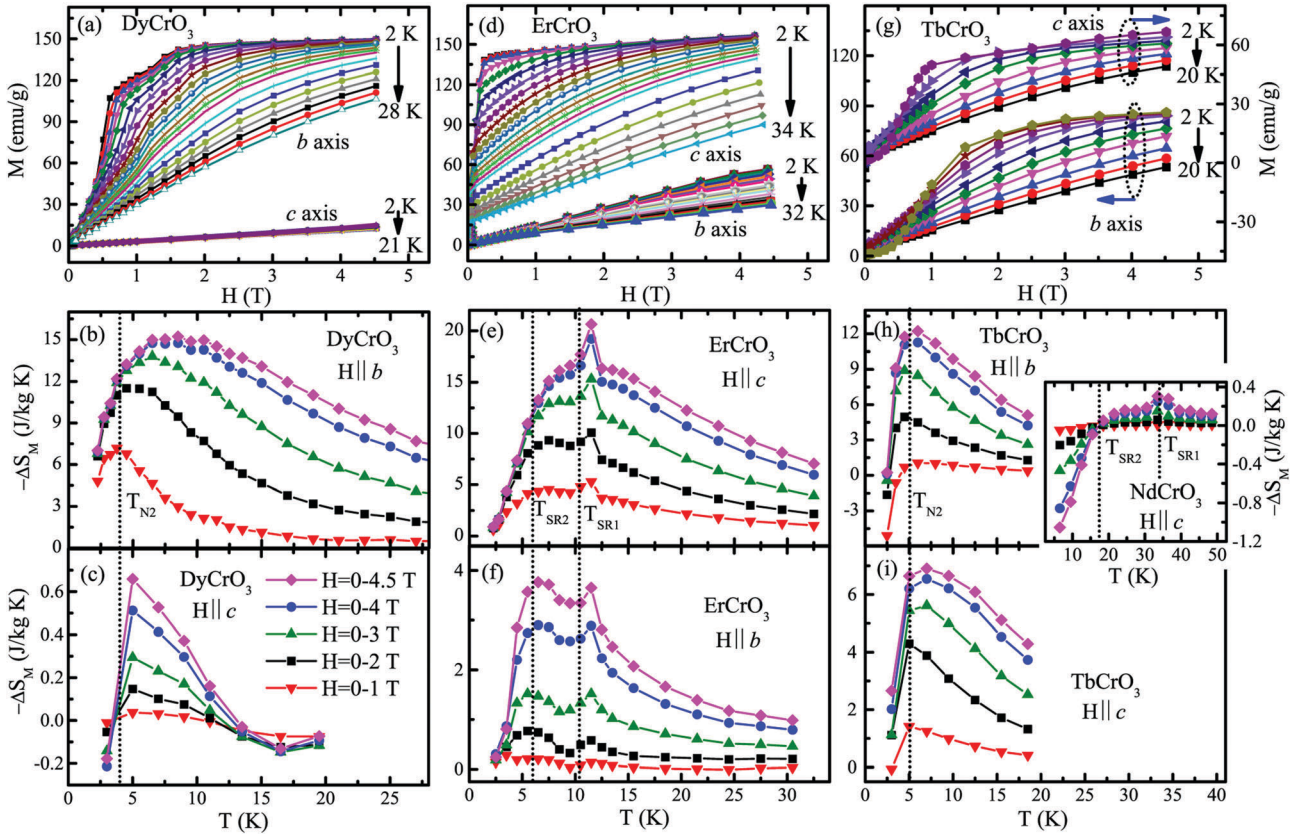

Fig. 7 Isothermal magnetization along different axes at different temperatures and the corresponding MC effect on $RCrO_3$ crystals.

ordering of R^{3+} spins in the temperature dependent $-\Delta S_M$ (Fig. 7), indicating a dominating role of the R–R or R–Cr magnetic interactions in the MC effect at low temperatures. In addition, an anomaly around the temperature T_{SR1} of spin reorientation of Cr^{3+}, where the Er^{3+} or Nd^{3+} spins also begin to rotate as a result of the R–Cr interaction, was also observed in $ErCrO_3$ or $NdCrO_3$ (Fig. 7). The sharp anomaly in the $-\Delta S_M$–T curves around T_{SR1} and T_{N2} in $ErCrO_3$ and $NdCrO_3$, respectively, is consistent with the first order nature of these two magnetic transitions, as clearly indicated by the sign change of the slope of the Arrott plot in Fig. S5 and S6 (ESI†).

Similar to $RFeO_3$ and $RMnO_3$,[5,7] the isostructural $RCrO_3$ polycrystalline samples were also reported to show ME and multiferroic behaviors.[13,14,16] In the present work, we focused on the possible ME effect around the magnetic transitions of the R^{3+} sublattice in the $RCrO_3$ single crystals. Fig. 8a shows the temperature dependent dielectric constant ε' along different axes for the $DyCrO_3$ crystal. The dielectric constant is normalized by the data at 30 K. It is clear that ε_c' shows a rapid upturn below T_{SR2}, while ε_a' and ε_b' decrease continuously. With further cooling, the ε' along all three axes exhibit a peak near the ordering temperature T_{N2} of the Dy^{3+} spins. The dielectric peak around T_{N2} along the c axis is much stronger than along the other two axes. This strong anisotropy in the ME effect resembles the magnetic anisotropy in the M–T curves induced by the R–Cr magnetic interaction (Fig. 2a). Below T_{N2}, ε_c' varies obviously with the applied magnetic field H (Fig. 8b). For the magnetodielectric measurement shown in Fig. 8(b) and the inset in it, the direction of the electric field is the same as that of the applied H. In the temperatures (*e.g.*, 12 K) between T_{N2} and T_{SR2}, the magnetodielectric effect becomes weaker (Fig. 8b). The smaller variations in ε_b' and larger variation in ε_c' with magnetic field are in contrast to the step-rise and linear behaviors in the M_b–H and M_c–H curves, respectively, below T_{SR2}. The larger magnetodielectric effect along the c axis than that along the b axis might be related to two factors. First, the electrical dipole induced by the Dy–Cr and/or Dy–Dy interaction at low temperatures might be parallel to the c axis. Second, the contribution to ε' from the Dy–Cr and/or Dy–Dy interactions along the c axis dominates over the interactions in the ab plane below T_{SR2}. As for the different behavior in H dependent M_c and ε_c', it might be due to the fact that the dielectric constant is more sensitive than the magnetization to the H-induced transition of the Dy–Cr and/or Dy–Dy interactions.

The steep upturn below T_{SR2} and sharp peak around T_{N2} in ε_c'–T can be significantly suppressed by applying a field of 3 T (inset in Fig. 8b). Note that the ordering (at T_{N2}) and induced ordering (at T_{SR1}/T_{SR2}) of the Dy^{3+} spins were also simultaneously suppressed by applying a high H (Fig. 4). These results clearly reveal an intrinsic ME effect in the $DyCrO_3$ crystal. Similarly, $RCrO_3$ with R = Nd, Tb also show a dielectric anomaly in the vicinity of the ordering (R = Tb) or induced ordering (R = Nd) temperature of R^{3+} spins (Fig. 9a and Fig. S7 in the ESI†). While in $ErCrO_3$, a dielectric anomaly occurred around the T_{SR1} at

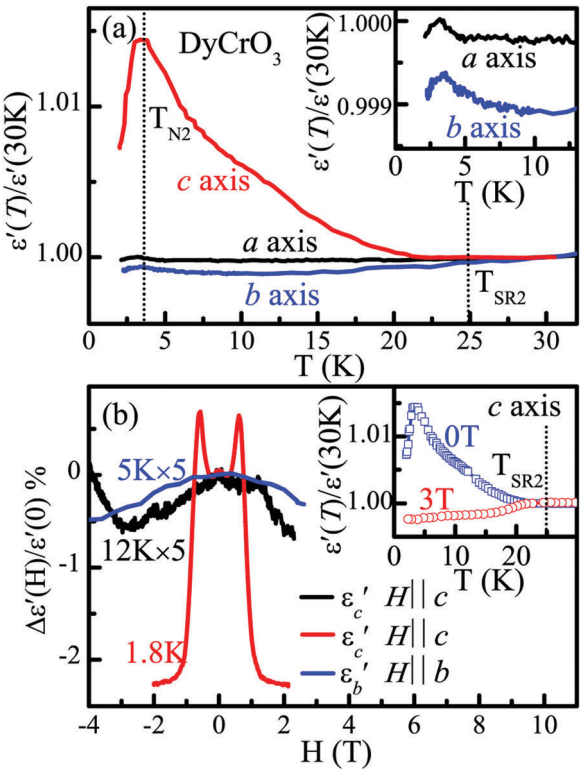

Fig. 8 (a) Dielectric constant scaled by the value of 30 K as a function of temperature along different axes for $DyCrO_3$ crystals. Inset is the magnification of the low T region. (b) Magnetodielectric effect for the b axis at 5 K and for the c axis at 1.8 and 12 K. Inset is the low-T ε_c'–T curves with H = 0 and 3 T, respectively.

which the Cr^{3+} spins reorient (Fig. 9b). These results clearly demonstrate a close relationship between the ME effect and the R–R or R–Cr magnetic interactions in the chromites.

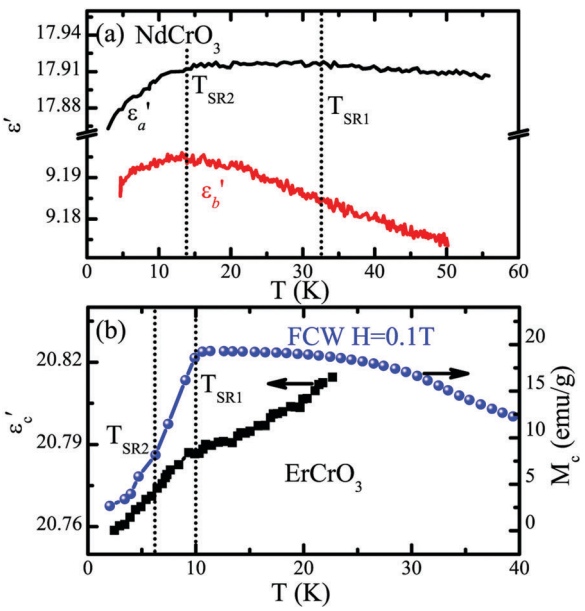

Fig. 9 Temperature dependence of dielectric constant and magnetization around T_{SR1} and T_{SR2} for $NdCrO_3$ (a) and $ErCrO_3$ (b) crystals.

However, the ME coupling in these chromites was not accompanied with multiferroicity below T_{SR1} or T_{N2}, as revealed by the absence of pyroelectric current (not shown here), while the ferroelectric transition around T_{N1} still needs further clarification due to the leakage problem. This behavior is very different from the isostructural $RFeO_3$ (R = Gd, Dy, *etc.*) systems,[5,6] and is also in contrast with previous results on polycrystalline chromites.[13,14] Now, we focus on the low temperature ME effect. According to the Lyddane–Sachs–Teller relation,[32] phonons with optical frequencies contributing much to ε' are coupled to a spin–spin correlation function. And indeed, the ME effect in chromites becomes stronger when R–R or R–Cr magnetic interactions are enhanced at low temperatures, and the close relationship between the ME effect and these interactions is clearly revealed as discussed above. Therefore, it is reasonable to ascribe the ME effect at low temperatures to the spin–phonon coupling in these chromites.[32,33]

4 Conclusions

In summary, we investigated in detail the magnetic, specific heat, ME, and MC properties in rare earth orthorchromite $RCrO_3$ (R = Dy, Nd, Tb, Er) single crystals synthesized using the flux method. We found some especially interesting new magnetic phase transitions related to the induced reorientation/ordering of rare earth spins in $RCrO_3$ (R = Dy, Nd, Er) and a multi-step like behavior in H-dependent M related to the relative spin orientation of Tb and Cr sublattices in the $TbCrO_3$ crystal. Large MC and rotating MC effects were observed in the vicinity of ordering or induced ordering temperatures of R^{3+} spins in the studied crystals. In addition, obvious ME effects related to the R–R, R–Cr, and Cr–Cr magnetic interactions were also observed in these $RCrO_3$ crystals. All the results suggest an important role of rare earth ions in the magnetic, MC and ME properties in the $RCrO_3$ systems.

Acknowledgements

This work was supported by the National Basic Research Program of China (2014CB931704) and the National Natural Science Foundation of China under Grant No. 11404339, 11374304 and 11274313 and the Joint Funds of the National Natural Science Foundation of China and the Chinese Academy of Sciences' Large-Scale Scientific Facility under Grant No. U1532152, U1432137 and U1432139. The work at SNU was supported by NRF, Korea through grants No. 2016K1A4A3914691 and 2010-0018300.

References

1 J. Shen, L.-D. Sun and C.-H. Yan, *Dalton Trans.*, 2008, 5687–5697.
2 S. Y. Dan'kov, A. M. Tishin, V. K. Pecharsky and K. A. Gschneidner, *Phys. Rev. B: Condens. Matter Mater. Phys.*, 1998, **57**, 3478–3490.
3 S. Sugimoto, *J. Phys. D: Appl. Phys.*, 2011, **44**, 064001.

4 K. A. Gschneidner Jr, V. K. Pecharsky and A. O. Tsokol, *Rep. Prog. Phys.*, 2005, **68**, 1479.
5 Y. Tokunaga, S. Iguchi, T. Arima and Y. Tokura, *Phys. Rev. Lett.*, 2008, **101**, 097205.
6 Y. Tokunaga, N. Furukawa, H. Sakai, Y. Taguchi, T. Arima and Y. Tokura, *Nat. Mater.*, 2009, **8**, 558–562.
7 T. Kimura, T. Goto, H. Shintani, K. Ishizaka, T. Arima and Y. Tokura, *Nature*, 2003, **426**, 55–58.
8 E. F. Bertaut, *Magnetism III*, Academic Press, New York, 1968.
9 L. H. Yin, J. Yang, X. C. Kan, W. H. Song, J. M. Dai and Y. P. Sun, *J. Appl. Phys.*, 2015, **117**, 133901.
10 S. Lei, L. Liu, C. Wang, C. Wang, D. Guo, S. Zeng, B. Cheng, Y. Xiao and L. Zhou, *J. Mater. Chem. A*, 2013, **1**, 11982–11991.
11 L. Yin, Y. Liu, S. Tan, B. Zhao, J. Dai, W. Song and Y. Sun, *Mater. Res. Bull.*, 2013, **48**, 4016–4021.
12 J. Mao, Y. Sui, X. Zhang, Y. Su, X. Wang, Z. Liu, Y. Wang, R. Zhu, Y. Wang, W. Liu and J. Tang, *Appl. Phys. Lett.*, 2011, **98**, 192510.
13 B. Rajeswaran, D. I. Khomskii, A. K. Zvezdin, C. N. R. Rao and A. Sundaresan, *Phys. Rev. B: Condens. Matter Mater. Phys.*, 2012, **86**, 214409.
14 B. Rajeswaran, P. Mandal, R. Saha, E. Suard, A. Sundaresan and C. N. R. Rao, *Chem. Mater.*, 2012, **24**, 3591–3595.
15 K. R. S. P. Meher, C. Martin, V. Caignaert, F. Damay and A. Maignan, *Chem. Mater.*, 2014, **26**, 830–836.
16 A. Ghosh, A. Pal, K. Dey, S. Majumdar and S. Giri, *J. Mater. Chem. C*, 2015, **3**, 4162–4167.
17 M. Shao, S. Cao, S. Yuan, J. Shang, B. Kang, B. Lu and J. Zhang, *Appl. Phys. Lett.*, 2012, **100**, 222404.
18 K. Sardar, M. R. Lees, R. J. Kashtiban, J. Sloan and R. I. Walton, *Chem. Mater.*, 2011, **23**, 48–56.
19 G. Catalan, *Appl. Phys. Lett.*, 2006, **88**, 102902.
20 B. M. Wanklyn, *J. Mater. Sci.*, 1972, **7**, 813–821.
21 R. Hornreich, *J. Magn. Magn. Mater.*, 1978, **7**, 280–285.
22 K. Tsushima, T. Tamaki and Y. Yamaguchi, *AIP Conf. Proc.*, 1975, **24**, 69–70.
23 N. Kojima, I. Tsujikawa, K. Aoyagi and K. Tsushima, *J. Phys. Soc. Jpn.*, 1985, **54**, 4804–4820.
24 K. Toyokawa, S. Kurita and K. Tsushima, *Phys. Rev. B: Condens. Matter Mater. Phys.*, 1979, **19**, 274–283.
25 K. R. S. Preethi Meher, A. Wahl, A. Maignan, C. Martin and O. I. Lebedev, *Phys. Rev. B: Condens. Matter Mater. Phys.*, 2014, **89**, 144401.
26 Y. Su, J. Zhang, L. Li, B. Li, Y. Zhou, D. Deng, Z. Chen and S. Cao, *Appl. Phys. A: Mater. Sci. Process.*, 2010, **100**, 73–78.
27 J.-L. Jin, X.-Q. Zhang, G.-K. Li, Z.-H. Cheng, L. Zheng and Y. Lu, *Phys. Rev. B: Condens. Matter Mater. Phys.*, 2011, **83**, 184431.
28 A. Midya, S. N. Das, P. Mandal, S. Pandya and V. Ganesan, *Phys. Rev. B: Condens. Matter Mater. Phys.*, 2011, **84**, 235127.
29 M. Balli, S. Jandl, P. Fournier and M. M. Gospodinov, *Appl. Phys. Lett.*, 2014, **104**, 232402.
30 V. Tkáč, A. Orendáčová, E. Čižmár, M. Orendáč, A. Feher and A. G. Anders, *Phys. Rev. B: Condens. Matter Mater. Phys.*, 2015, **92**, 024406.
31 Y.-J. Ke, X.-Q. Zhang, H. Ge, Y. Ma and Z.-H. Cheng, *Chin. Phys. B*, 2015, **24**, 037501.
32 R. H. Lyddane, R. G. Sachs and E. Teller, *Phys. Rev.*, 1941, **59**, 673–676.
33 G. Lawes, A. P. Ramirez, C. M. Varma and M. A. Subramanian, *Phys. Rev. Lett.*, 2003, **91**, 257208.

